Published in final edited form as:
Clin Cancer Res. 2014 March 1; 20(5): 1288–1297. doi:10.1158/1078-0432.CCR-13-2611.

Tumorgrafts as *in vivo* surrogates for women with ovarian cancer

S. John Weroha[1], **Marc A. Becker**[1], **Sergio Enderica-Gonzalez**[1], **Sean Harrington**[1], **Ann L Oberg**[2], **Matthew J. Maurer**[2], **Sarah E. Perkins**[2], **Mariam Al Hilli**[3], **Kristina A. Butler**[3], **Sarah McKinstry**[1], **Stephanie Fink**[4], **Robert Jenkins**[4], **Xiaonan Hou**[1], **Kim Kalli**[1], **Karin Goodman**[1], **Jann Sarkaria**[5], **Beth Karlan**[6], **Amanika Kumar**[3], **Scott H. Kaufmann**[1,7], **Lynn C. Hartmann**[1], and **Paul Haluska**[1,*]

[1]Department of Oncology, Mayo Clinic, Rochester, MN, USA

[2]Division of Biomedical Statistics and Informatics within the Department of Health Sciences Research, Mayo Clinic, Rochester, MN, USA

[3]Division of Gynecologic Surgery, Mayo Clinic, Rochester, MN, USA

[4]Laboratory Medicine and Pathology, Mayo Clinic, Rochester, MN, USA

[5]Department of Radiation Oncology, Mayo Clinic, Rochester, MN, USA

[6]Women's Cancer Program at the Samuel Oschin Cancer Institute, Cedars-Sinai Medical Center, Los Angeles, CA, USA

[7]Department of Molecular Pharmacology and Experimental Therapeutics, Mayo Clinic, Rochester, MN, USA

Abstract

Purpose—Ovarian cancer has a high recurrence and mortality rate. A barrier to improved outcomes includes a lack of accurate models for preclinical testing of novel therapeutics.

Experimental Design—Clinically-relevant, patient-derived tumorgraft models were generated from sequential patients and the first 168 engrafted models are described. Fresh ovarian, primary peritoneal, and fallopian tube carcinomas were collected at the time of debulking surgery and injected intraperitoneally into severe combined immunodeficient mice.

Results—Tumorgrafts demonstrated a 74% engraftment rate with microscopic fidelity of primary tumor characteristics. Low-passage tumorgrafts also showed comparable genomic aberrations with the corresponding primary tumor and exhibit gene set enrichment of multiple ovarian cancer molecular subtypes, similar to patient tumors. Importantly, each of these tumorgraft models are annotated with clinical data and for those that have been tested, response to platinum chemotherapy correlates with the source patient.

Conclusions—Presented herein is the largest known living tumor bank of patient-derived, ovarian tumorgraft models that can be applied to the development of personalized cancer treatment.

[*]Correspondence should be addressed to: Dr. Paul Haluska MD, PhD, Division of Medical Oncology, Mayo Clinic College of Medicine, 200 First St. SW, Rochester, MN 55905, haluska.paul@mayo.edu.

Authors' Disclosure of Potential Conflicts of Interests: None

Keywords

Severe combined immunodeficient (SCID) mouse; xenograft; intraperitoneal; heterotransplantation; orthotopic; preclinical

Introduction

Ovarian cancer (OC) develops in an estimated 22,240 women in the US annually (1) and most commonly presents with advanced stage, which has a high recurrence rate (2). Although incremental advances in chemotherapy over the last four decades have improved median survival, the cure rate is essentially unchanged (3) and OC remains the most lethal gynecologic malignancy. An important barrier to achieving better outcomes for these patients is a lack of *in vivo* models that accurately reflect the diverse histology and molecular biology of primary tumors and predict their response to treatment.

Cell lines and cell-line-derived xenograft models have contributed significantly to our current understanding of OC development. However, it is well known that *in vitro* models are prone to culture-induced genotypic and phenotypic alterations that can diverge from the parent tumor (4, 5). Thus the extrapolation of *in vitro* data to patient outcomes and response to therapy is of questionable utility. Indeed, the most frequently used OC cell lines are significantly divergent from the molecular characteristics of OC patients (6) and may partially explain the lack of evidence supporting the use of *in vitro* drug sensitivity assays (7). Although xenograft models derived from human cell lines are an improvement (8–10), they are ultimately subject to many of the same limitations.

Heterotransplantation of fresh human tumors, also referred to as “tumorgrafts”, may more-accurately recapitulate the primary patient tumor. When maintained under conditions of low passage *in vivo*, such models maintain histologic (11–13) and genomic (14) fidelity. As a result, tumorgrafts may act as better surrogates for patients and more accurately predict responses to treatment. As proof of principle, tumorgraft models developed for sarcoma, melanoma, and adenocarcinoma demonstrated strong correlation with the patient experience when tumorgraft response was used to guide treatment for patients (15). Although ovarian tumorgrafts have been used to study the efficacy of targeted therapies in molecularly-defined subgroups, such as BRCA1/2 mutated (14, 16) or HER2 up-regulated (17, 18) OC, a prospective tumorgraft-guided study has not yet been reported for women with OC. To generate the patient surrogates for such studies, we now demonstrate the feasibility of large-scale intraperitoneal engraftment of ovarian tumor tissues in severe combined immunodeficient (SCID) mice and show their pathologic, molecular, and treatment-responsive similarities to the source patients.

Methods

Tumor engraftment and cryo-preservation

Fresh tissues from consenting patients with ovarian, primary peritoneal, or fallopian tube cancer were collected at the time of debulking surgery at Mayo Clinic, Rochester. All biospecimens were coded with a patient heterotransplant (PH) number to protect patient identity but also maintain a restricted link to clinical data in accordance with the Mayo Clinic Institutional Review Board. Frozen sections of all specimens were first analyzed by a pathologist to make the diagnosis of cancer and 3 cm^3 of non-necrotic adjacent malignant tissue was procured by clinical staff with specialized training in gross dissection. Tumors were minced on ice and in limiting volumes of ice-cold McCoy’s media (#10-050-CV, MediaTech). Approximately 0.3–0.5 cc of tumor slurry was mixed with 1:1 McCoy’s media

and injected intraperitoneally in at least three female SCID mice (C.B.-17/IcrHsd-*Prkdc*^{scid} *Lyst*^{bg}; Harlan Labs), in accordance with the Mayo Clinic Institutional Animal Care and Use Committee. Moribund mice with tumor were sacrificed and to maintain each tumorgraft model as low-passage, tumor from the initial founder mouse/mice is expanding with a single passage into 10+ mice in order to generate sufficient tumor volume for banking and future experiments. If the founder tumorgraft volume is insufficient, a pre-expansion amplification of tumor volume may be necessary in a small cohort of mice. Cryopreserved tumors are minced and stored 1:1 in freezing media (39% FBS, 10% DMSO, 1% penicillin/streptomycin in McCoy's media) overnight at −80°C then in liquid nitrogen indefinitely. Ascites harvested from moribund mice was collected by sedated paracentesis prior to necropsy and red blood cells were lysed using ACK buffer (NH4Cl 0.15 M, KHCO3 10.0 mM, Na2EDTA 0.1 mM); cells were viably frozen as above.

Tissue processing and immunohistochemistry

Tissues collected from mice or patients were fixed overnight in buffered formalin (Fisher Scientific, #23-011-120) and processed in the tissue core facility at Mayo Clinic, AZ. Deparaffinized and rehydrated 5–6 μm sections were unmasked for 15 min in EDTA Buffer (1mM EDTA, 0.05% Tween 20, pH 8.0) at 95–99°C. Primary antibodies purchased from Life Technologies (pan-cytokeratin clone AE1/AE3 at 1:300 and Vimentin V9 at 1:2000) and Dako North America (Ki67 clone MIB1 at 1:600, CD45 clone 2B11+PD7/26 at 1:500) were incubated overnight at 4°C. Secondary antibody (Cell Signaling, SignalStain Boost IHC detection system #8125S) was applied for 30–60 min at room temperature. Chromogenic detection of protein expression was determined in the presence of DAB (BioCare, Betazoid DAB) and visualized by light microscopy.

In vivo CA125 measurements

Whole blood was collected by sedated cardiac puncture from moribund mice bearing tumorgrafts and at necropsy. Serum was collected after a 30–60 min incubation at room temperature, centrifugation at >13,000 g for 10 min, and stored at −80°C. Sera (100 μL) were assayed for human CA125 using an ELISA kit according to the manufacturer's protocol (#CA125T, Calbiotech). The standard curve (r^2=0.994) and all reference controls were within the expected range. All patient samples were analyzed by the Mayo Clinic central clinical laboratory.

Microarray and array comparative genomic hybridization (aCGH)

RNA and DNA was simultaneously extracted following the manufacturers protocol for Qiagen AllPrep DNA/RNA mini Kit (#80204). Nucleic acid concentration and purity was determined on a Thermo Scientific NanoDrop 2000c UV-Vis Spectrophotometer. Total tumorgraft RNA was analyzed by Affymetrix HG U133 plus 2.0 arrays at the Mayo Medical Genome Facility according to the manufacturer's protocol.

To assess for genomic gains and losses, aCGH was performed on the Agilent Human Genome CGH microarray kit 244A using matched-patient reference genomic DNA as previously described (19). Briefly, genomic DNA was collected as above and 1 microgram of test (tumor) and reference (matched patient germline) DNA was labeled with Cy5 and Cy3, respectively, by random priming PCR, hybridized over 24 hrs at 65°C, and analyzed with Agilent Technologies Genomic Workbench 6.5 Lite Edition software. Gains and losses were defined as >4 regional probes with an absolute average log ratio of 0.26 for the region, which equates to <1.67 gene copies for losses and >2.4 gene copies for gains.

Gene expression arrays were preprocessed and normalized by robust multi-chip analysis (RMA)(20). For differential gene expression studies, platinum-sensitive vs. platinum-

resistant tumorgrafts were compared using the linear models and empirical Bayes methods that share information across genes to estimate variance (LIMMA)(21) and visualized with Cluster (22) and Java TreeView (23). The criteria for differential expression was defined as fold change ≥5-fold and p-value of <0.01. For molecular subtyping, single sample gene set enrichment analysis (ssGSEA) was applied to 36 tumorgrafts using the CLassification of OVARian cancer (CLOVAR) gene set and Normalized Enrichment Scores (NES) were derived as previously described (24). The degree of similarity across tumorgrafts was defined by the Pearson correlation coefficient between NES profiles.

In vivo imaging

Mouse abdominal fur was removed with Nair Sensitive Skin (Church & Dwight Co., Inc.). Aplicare sterile jelly lubricant (#82-280, Cardinal Healthcare) was applied to bare skin and an L-25× 13-6 MHz linear transducer with a SonoSite S-Series Ultrasound was used to capture weekly images for analysis of tumor cross-sectional area in ImageJ 1.46 platform independent software (25).

Tumorgraft chemotherapy treatment

Mice with 0.5–1 cm tumors were randomized to either IP saline or carboplatin (#61703-360-18)/paclitaxel (#55390-304-05) from NOVAPLUS at 50 mg/kg and 15 mg/kg, respectively, on days 1, 8, 15, and 22 as described (26). The primary endpoint was change in tumor size relative to day 1.

Statistical analysis

Time to engraftment and engraftment rate was determined using a cumulative incidence approach to account for models still under observation for determination of engraftment. Comparisons between engraftment status and patient characteristics were assessed using chi-squared tests and Wilcoxon rank-sum tests. Spearman's correlation was used to assess association between continuous variables. Association between engraftment status and overall survival for the patient were assessed using Kaplan-Meier curves and Cox proportional hazards models; overall survival was defined as time from ovarian cancer to death or date of last follow-up.

Results

Clinical characteristics of tumorgrafts

Ovarian, primary peritoneal (PP), or fallopian tube tumors were collected at the time of surgery from patients at Mayo Clinic (Rochester, MN) and injected intraperitoneally into female SCID mice under and an approved Institutional Animal Care and Use Committee protocol. 241 models have been injected through 12/31/2012; 168 models have engrafted (Table 1), 46 models failed, and 27 are still under assessment (censored for evaluation) at the time of this publication. After an initial pilot study to determine optimal conditions, the engraftment rate is 74% (Fig. 1A). Patient data are associated with each tumorgraft in accordance with Health Insurance Portability and Accountability Act regulations and maintained by the Mayo Clinic Ovarian Tumor Repository. Basic information such as stage and grade are abstracted along with more detailed data such as chemotherapy type and number of cycles, recurrence-free and overall survival, and CA125 levels over time. Histologic diversity of tumorgrafts is reflective of ovarian cancer patients with serous comprising the most common histologic subtype (Table 1). Mixed histology was seen and rare subtypes, carcinosarcoma and transitional cell, have engrafted. Successful mouse engraftment was associated with adverse patient characteristics such as advanced stage (p=0.049), high-grade tumors (p=0.00087), and presence of ascites (p= 0.00091). Although

ascites was more common in serous PP (15/19) relative to serous ovarian (43/71) tumorgrafts, consistent with other studies (27–30), this difference was not significant (p = 0.2255) and the relative frequency of ovarian and PP tumors in tumorgrafts (3.74 to 1) was comparable to all patients consenting for this study (3.89 to 1). In addition, patients whose tumors successfully engrafted in mice had inferior overall survival (HR=2.14, 95% CI: 0.90–5.08, p=0.059) relative to patients whose tumors did not successfully engraft (Fig. 1B).

Recapitulation of metastatic pattern in tumorgrafts

Tumorgraft models reproduce clinically relevant complications of ovarian cancer. The most common site of engraftment is in the pelvis but 46% of models will have involvement of the bowel, mesentery, visceral pleura of liver, spleen, diaphragm, or omentum. Intraperitoneal dysfunction, such as bowel obstruction (Fig. 1C, left), is observed along with mesenteric engraftment (Fig. 1C, right), which may not be obstructive but can still cause weight loss in a near-moribund mouse. Of the 17 models which developed ascites in at least one mouse, 70.6% were derived from patients who had ascites at the time of debulking surgery. Tumorgraft ascites was typically bloody or serosanguineous. When normal mouse peritoneum (Fig. 1D, left) was compared to mice developing ascites, carcinomatosis is evident by innumerable explants forming a continuous sheet of malignant cells (Fig. 1D, center). Discrete masses often did not form in this setting but aggregates of cells in clusters or spherules (Fig. 1D, right) are apparent within ascitic fluid and carry malignant potential when passaged. As a pilot, 0.2 mL of fresh ascites from one mouse produced carcinomatosis and ascites in 3 out of 3 mice within 44–67 days.

Microscopic similarity between patients and tumorgrafts

In order to demonstrate similarity between tumorgrafts and their primary tumors, low-passage tissues were compared to initial surgical specimens. The glandular characteristic of adenocarcinoma was conserved, along with the relative proliferation index (Fig. 2A and Supplemental Fig. 1). Expression of pan-cytokeratin confirmed the epithelial origin each tumorgraft, which is necessary because SCID mice can develop spontaneous lymphomas (31). Although tumor-associated lymphocytes (TAL) are common in primary tumors (32), CD45-positive cells did not frequently co-heterotransplant with epithelial tumors (Fig. 2A). However, persistent CD45-positive cells were observed in a subset of tumorgraft models: PH040 and PH055 harvested 110 and 78 days, respectively, after injection into mice (Supplemental Fig. 2).

To determine if tumorgraft microenvironment mimics source tumors, stromal composition was estimated with ImageJ, as previously described (33). This was performed in eight models by selecting non-epithelial tissue areas which were negative for pan-CK expression, and plotting the percent area per field in patient tissue versus tumorgraft tissue (Fig. 2B). Strong correlation was seen in percent stroma composition with a Spearman r = 0.7381 (p=0.0458), suggesting a tendency for some tumors to induce stroma *de novo* as the epithelial component expanded (Fig. 2C). When patient and tumorgraft tissues were evaluated for expression of human vimentin using an antibody with no reactivity against mouse protein (34), patient stroma stained strongly while tumorgraft stroma did not, indicating that the stroma is murine and a subset of tumorgrafts maintain a propensity to recapitulated the source tumor microenvironment (Supplemental Fig. 2).

Genomic aberrations and molecular subtyping of tumorgrafts

Array comparative genomic hybridization (aCGH) was performed on 41 tumorgraft models. To demonstrate the fidelity of aberrations between source patients and their resultant tumorgrafts, aCGH was performed in two tumorgraft models from different patient tumors. The results show marked overlap in genetic gains and losses between the patient tumor and

corresponding tumorgraft (Fig. 3A). In addition, commonly gained/lost genes in ovarian cancer, as determined by gene copy number analysis of 489 ovarian serous carcinomas from The Cancer Genome Atlas Research Network (TCGA)(35), are seen in 41 tumorgraft models (Fig. 3B and Supplemental Fig. 3).

Ovarian cancer molecular subtypes have been proposed, based on global gene expression analysis (36), which was later validated in an independent dataset supporting four distinct molecular subtypes (differentiated, proliferative, immunoreactive, and mesenchymal) (35). More recent evidence suggests that individual ovarian tumors are markedly heterogeneous in terms of subtype enrichment (24). Similar to patient tumors, early-passage tumorgrafts (n=36) do not clearly classify into a specific subtype, but do exhibit gene set enrichment of multiple ovarian cancer subtypes and high correlation within subsets (Fig. 3C).

Limited utility of clinical CA125 in sera of mice bearing tumorgrafts

In vivo monitoring of tumor burden is necessary to assess real-time response to therapy. Given its clinical utility, CA125 has been considered as a biomarker of response during treatment experiments with tumorgraft models (11). To investigate this further, a pilot study with sera from eight models was conducted. All mice were near moribund with tumor, but not in excess of standard animal care and use regulations, in order to maximize circulating CA125. All models were derived from patients with high pre-operative CA125 levels (median 1507, range 276 to 3130). Only three models (PH013, PH015, and PH038) had CA125 levels above the limit of detection, despite having maximum tumor burden (Supplemental Fig. 4). Even then, CA125 levels in mice were only modestly elevated.

Correlation of response between patient and tumorgraft

To assess the clinical relevance of these models, response to platinum-doublet chemotherapy was investigated. Patients PH037, PH053, PH069 and PH070 had either platinum refractory or resistant cancer, defined as tumor progression during or within 6 months of completing chemotherapy, respectively (Supplemental Table 1). PH013, PH015, PH039, PH077, and PH080 were derived from platinum-sensitive patients. Although patient PH077 clinically recurred 4.43 months after completing chemotherapy, she was still considered platinum sensitive because post-operative complications necessitated treatment delays and dose modifications, which led to suboptimal adjuvant treatment; after recurrence, she was subsequently treated with nine cycles of carboplatin/paclitaxel and achieved a complete response by CA125 and CT scan, indicative of platinum-sensitive disease. All nine tumorgraft models were heterotransplanted in SCID mice. Since tumor diameter accounts for only one dimension of growth, weekly cross-sectional area was measured by transabdominal ultrasonography to determine response. Tumor tissue (hypo-echoic in mouse abdomen) can be discriminated from surrounding bowel/stool (Fig. 4A). Ultrasound highly correlated with traditional caliper-based measurements when both modalities were compared at necropsy (Fig. 4B). Representative ultrasound images show decreased tumor area and echogenicity in a sensitive tumorgraft while a resistant tumorgraft demonstrated no change in the target mass but a new (non-target) tumor grew on treatment (Fig. 4C). Saline-treated controls grew without regression. Nine of nine tumorgrafts (100%) demonstrated *in vivo* platinum responses reflective of the respective patient's clinical response. After four weeks of carboplatin/paclitaxel as described in the Methods, PH037 (n=9), PH053 (n=6), PH069 (n=8), and PH070 (n=8) exhibited tumor growth while PH013 (n=9), PH015 (n=6), PH039 (n=6), PH077 (n=10), and PH080 (n=7) regressed (Fig. 5A). When untreated tumors were analyzed by Affymetrix for differential gene expression, two distinct patterns are apparent and are suggestive of a molecular difference between platinum-sensitive and -resistant tumorgrafts (Fig. 5B).

Discussion

The models presented herein comprise the largest published bank of human ovarian, primary peritoneal, and fallopian tube tumorgrafts. They recapitulate key clinical and molecular characteristics of the primary tumors and are molecularly relevant. Responses to carboplatin and paclitaxel *in vivo* correlate well with the corresponding patient's clinical response. Although the most common pathologic subtypes are represented, the breadth of the engrafted models include less common subtypes, such as carcinosarcomas and transitional cell ovarian cancer, providing an opportunity to test therapies for subtypes with limited options. Taken together, these tumorgrafts are valuable surrogates for ovarian cancer patients.

A major strength of these tumorgrafts is the clinical data that accompanies each model. Tumorgrafts can be selected for preclinical testing of novel therapeutics in a clinically-defined subset of OC patient surrogates (such as those with known *BRCA* mutations or platinum-resistant disease). Moreover, the availability of pre- and post-treatment tissue for correlative studies would obviate the need for invasive procedures in patients. In addition, actual tumor response to treatment can be determined *in vivo* without relying on clinical outcomes to approximation clinical benefit, such as the platinum-free interval used to define clinical platinum resistance. This is an imprecise surrogate of response and may incorrectly deny a patient from, or subject a patient to, platinum therapy (37). PH077 above is a case in point and supports the use of patient-derived OC surrogates for preclinical testing of standard and novel therapeutics. The feasibility of maintaining a viably-frozen tumor bank is demonstrated in a high rate of engraftment after thawing. Twenty-two models have been pulled from frozen stocks and all were successfully reconstituted in mice. Across all models, the re-engraftment rate was 97.7% (n= 307).

The applicability of these tumorgraft models to OC is demonstrated by the molecular diversity seen between models, a reflection of the diversity seen in primary patient tumors (35, 36). The observation that individual ovarian cancers exhibit characteristics of multiple subtypes underscores the difficulty with assigning a single molecular subtype to a tumor as this does not fully account for the genetic complexity that may complicate therapeutic response. Designing future studies to target specific pathways associate with enriched molecular subtypes gives rise to the potential for personalized therapies and the models presented herein provide a mechanism to accomplish this goal. They may also help investigators design better clinical trials through discovery of predictive biomarker as well as testing combination therapies to find optimal drug doublets or triplets. As proof of principle, all nine tumorgraft models responded to chemotherapy commensurate to the corresponding patient's clinical response and distinct gene expression patterns differentiate platinum-resistant and –sensitive tumors. The molecular mechanisms of resistance are multifactorial and studies are currently underway to better understand the specific genes and/or pathways involved.

The histologic conservation of primary tumor morphology and proliferation rate is consistent with other orthotopic tumorgraft models of ovarian cancer (10–14, 16, 38, 39). Maintenance of each model entirely *in vivo* would appear to be an important process since some ovarian tumorgrafts, which are initially established in mice but subsequently cultured *in vitro*, may no longer resemble the primary tumor and have altered response to chemotherapy (6, 38). Although TAL may play a role in human OC progression, their significance in tumorgrafts remains to be seen. Human lymphocytes have been reported in other tumorgraft models (11, 13) but the uncommon occurrence in the present study suggests they are not necessary for engraftment or maintenance of the tumorgrafts.

Accurate assessment of *in vivo* tumor response is central to tumorgraft-based experiments and SCID mice pose unique challenges in this regard. For instance, small animal CT, PET, or MRI scanners may not be conveniently located in an animal barrier room, exposing SCID mice to unacceptable infection risk. In contrast, portable ultrasound overcomes these limitations and also avoids the need for general anesthesia while providing accurate pre- and post-treatment tumor measurements, thereby allowing each animal to function as its own reference. We recognize that ultrasound is not used clinically since intraperitoneal tumors can be obscured by bowel and subcutaneous adipose tissue but mice are not limited by similar structural obstacles or large surface area as seen in the human intraperitoneal cavity. Moreover, when ultrasound measurements were compared to traditional caliper measurements at necropsy, correlation was strong. On the other hand, serial CA125 measurements have been proposed for ovarian tumorgrafts (11) but in our series, low sensitivity was limiting. This finding is consistent with the observation that human peritoneum is a source of serum CA125(40) and its elevation in some patients may reflect peritoneal irritation from tumor burden, which is not measurable in mice using standard clinical assays (41).

In summary, ovarian cancer remains the most lethal malignancy in women but there is hope that novel therapies or combinations of existing therapies will extend disease-free and overall survival. The development of accurate surrogates for OC patients enables investigators to discover new treatments and advance the vision of individualized therapy. As this tumor bank continues to grow, we hope to gain a better understanding of the mechanisms involved in chemotherapy resistance and develop new strategies to overcome barriers to better outcomes in our patients.

Supplementary Material

Refer to Web version on PubMed Central for supplementary material.

Acknowledgments

Support: This research was supported by the following: United States National Institutes of Health Grants T32 DK07352 and CA136393, Mayo Clinic SPORE in Ovarian Cancer.

References

1. Siegel R, Naishadham D, Jemal A. Cancer statistics, 2013. CA: a cancer journal for clinicians. 2013; 63:11–30. [PubMed: 23335087]
2. Horner, MJ.; Ries, LAG.; Krapcho, M.; Neyman, N.; Aminou, R.; Howlader, N., et al. SEER Cancer Statistics Review, 1975–2006. National Cancer Institute; Bethesda, MD: 2009.
3. Barnholtz-Sloan JS, Schwartz AG, Qureshi F, Jacques S, Malone J, Munkarah AR. Ovarian cancer: changes in patterns at diagnosis and relative survival over the last three decades. Am J Obstet Gynecol. 2003; 189:1120–7. [PubMed: 14586365]
4. Hausser HJ, Brenner RE. Phenotypic instability of Saos-2 cells in long-term culture. Biochem Biophys Res Commun. 2005; 333:216–22. [PubMed: 15939397]
5. Wenger SL, Senft JR, Sargent LM, Bamezai R, Bairwa N, Grant SG. Comparison of established cell lines at different passages by karyotype and comparative genomic hybridization. Biosci Rep. 2004; 24:631–9. [PubMed: 16158200]
6. Domcke S, Sinha R, Levine DA, Sander C, Schultz N. Evaluating cell lines as tumour models by comparison of genomic profiles. Nat Commun. 2013; 4:2126. [PubMed: 23839242]
7. Karam AK, Chiang JW, Fung E, Nossov V, Karlan BY. Extreme drug resistance assay results do not influence survival in women with epithelial ovarian cancer. Gynecologic oncology. 2009; 114:246–52. [PubMed: 19500821]

8. Langdon SP, Hendriks HR, Braakhuis BJ, Pratesi G, Berger DP, Fodstad O, et al. Preclinical phase II studies in human tumor xenografts: a European multicenter follow-up study. Ann Oncol. 1994; 5:415–22. [PubMed: 8075048]
9. Ward BG, Wallace K, Shepherd JH, Balkwill FR. Intraperitoneal xenografts of human epithelial ovarian cancer in nude mice. Cancer research. 1987; 47:2662–7. [PubMed: 3567897]
10. Massazza G, Tomasoni A, Lucchini V, Allavena P, Erba E, Colombo N, et al. Intraperitoneal and subcutaneous xenografts of human ovarian carcinoma in nude mice and their potential in experimental therapy. Int J Cancer. 1989; 44:494–500. [PubMed: 2777413]
11. Bankert RB, Balu-Iyer SV, Odunsi K, Shultz LD, Kelleher RJ Jr, Barnas JL, et al. Humanized mouse model of ovarian cancer recapitulates patient solid tumor progression, ascites formation, and metastasis. PLoS One. 2011; 6:e24420. [PubMed: 21935406]
12. Elkas JC, Baldwin RL, Pegram M, Tseng Y, Slamon D, Karlan BY. A human ovarian carcinoma murine xenograft model useful for preclinical trials. Gynecol Oncol. 2002; 87:200–6. [PubMed: 12477452]
13. Xu Y, Silver DF, Yang NP, Oflazoglu E, Hempling RE, Piver MS, et al. Characterization of human ovarian carcinomas in a SCID mouse model. Gynecol Oncol. 1999; 72:161–70. [PubMed: 10021295]
14. Press JZ, Kenyon JA, Xue H, Miller MA, De Luca A, Miller DM, et al. Xenografts of primary human gynecological tumors grown under the renal capsule of NOD/SCID mice show genetic stability during serial transplantation and respond to cytotoxic chemotherapy. Gynecol Oncol. 2008; 110:256–64. [PubMed: 18547621]
15. Hidalgo M, Bruckheimer E, Rajeshkumar NV, Garrido-Laguna I, De Oliveira E, Rubio-Viqueira B, et al. A pilot clinical study of treatment guided by personalized tumorgrafts in patients with advanced cancer. Molecular cancer therapeutics. 2011; 10:1311–6. [PubMed: 21673092]
16. Kortmann U, McAlpine JN, Xue H, Guan J, Ha G, Tully S, et al. Tumor growth inhibition by olaparib in BRCA2 germline-mutated patient-derived ovarian cancer tissue xenografts. Clinical cancer research : an official journal of the American Association for Cancer Research. 2011; 17:783–91. [PubMed: 21097693]
17. Faratian D, Zweemer AJ, Nagumo Y, Sims AH, Muir M, Dodds M, et al. Trastuzumab and pertuzumab produce changes in morphology and estrogen receptor signaling in ovarian cancer xenografts revealing new treatment strategies. Clinical cancer research : an official journal of the American Association for Cancer Research. 2011; 17:4451–61. [PubMed: 21571868]
18. Cao Y, Marks JD, Marks JW, Cheung LH, Kim S, Rosenblum MG. Construction and characterization of novel, recombinant immunotoxins targeting the Her2/neu oncogene product: in vitro and in vivo studies. Cancer research. 2009; 69:8987–95. [PubMed: 19934334]
19. Cen L, Carlson BL, Schroeder MA, Ostrem JL, Kitange GJ, Mladek AC, et al. p16-Cdk4-Rb axis controls sensitivity to a cyclin-dependent kinase inhibitor PD0332991 in glioblastoma xenograft cells. Neuro-oncology. 2012; 14:870–81. [PubMed: 22711607]
20. Irizarry RA, Hobbs B, Collin F, Beazer-Barclay YD, Antonellis KJ, Scherf U, et al. Exploration, normalization, and summaries of high density oligonucleotide array probe level data. Biostatistics. 2003; 4:249–64. [PubMed: 12925520]
21. Smyth GK, Speed T. Normalization of cDNA microarray data. Methods. 2003; 31:265–73. [PubMed: 14597310]
22. Eisen MB, Spellman PT, Brown PO, Botstein D. Cluster analysis and display of genome-wide expression patterns. Proc Natl Acad Sci U S A. 1998; 95:14863–8. [PubMed: 9843981]
23. Saldanha AJ. Java Treeview--extensible visualization of microarray data. Bioinformatics. 2004; 20:3246–8. [PubMed: 15180930]
24. Verhaak RG, Tamayo P, Yang JY, Hubbard D, Zhang H, Creighton CJ, et al. Prognostically relevant gene signatures of high-grade serous ovarian carcinoma. J Clin Invest. 2013; 123:517–25. [PubMed: 23257362]
25. Schneider CA, Rasband WS, Eliceiri KW. NIH Image to ImageJ: 25 years of image analysis. Nat Methods. 2012; 9:671–5. [PubMed: 22930834]
26. Staflin K, Jarnum S, Hua J, Honeth G, Kannisto P, Lindvall M. Combretastatin A-1 phosphate potentiates the antitumor activity of carboplatin and paclitaxel in a severe combined

immunodeficiency disease (SCID) mouse model of human ovarian carcinoma. Int J Gynecol Cancer. 2006; 16:1557–64. [PubMed: 16884365]

27. Barda G, Menczer J, Chetrit A, Lubin F, Beck D, Piura B, et al. Comparison between primary peritoneal and epithelial ovarian carcinoma: a population-based study. Am J Obstet Gynecol. 2004; 190:1039–45. [PubMed: 15118638]
28. Halperin R, Zehavi S, Langer R, Hadas E, Bukovsky I, Schneider D. Primary peritoneal serous papillary carcinoma: a new epidemiologic trend? A matched-case comparison with ovarian serous papillary cancer. Int J Gynecol Cancer. 2001; 11:403–8. [PubMed: 11737473]
29. Jaaback KS, Ludeman L, Clayton NL, Hirschowitz L. Primary peritoneal carcinoma in a UK cancer center: comparison with advanced ovarian carcinoma over a 5-year period. Int J Gynecol Cancer. 2006; 16 (Suppl 1):123–8. [PubMed: 16515579]
30. Killackey MA, Davis AR. Papillary serous carcinoma of the peritoneal surface: matched-case comparison with papillary serous ovarian carcinoma. Gynecol Oncol. 1993; 51:171–4. [PubMed: 8276289]
31. Custer RP, Bosma GC, Bosma MJ. Severe combined immunodeficiency (SCID) in the mouse. Pathology, reconstitution, neoplasms. Am J Pathol. 1985; 120:464–77. [PubMed: 2412448]
32. Hwang WT, Adams SF, Tahirovic E, Hagemann IS, Coukos G. Prognostic significance of tumor-infiltrating T cells in ovarian cancer: a meta-analysis. Gynecol Oncol. 2012; 124:192–8. [PubMed: 22040834]
33. Papadopulos F, Spinelli M, Valente S, Foroni L, Orrico C, Alviano F, et al. Common tasks in microscopic and ultrastructural image analysis using ImageJ. Ultrastruct Pathol. 2007; 31:401–7. [PubMed: 18098058]
34. Bohn W, Wiegers W, Beuttenmuller M, Traub P. Species-specific recognition patterns of monoclonal antibodies directed against vimentin. Exp Cell Res. 1992; 201:1–7. [PubMed: 1612114]
35. Integrated genomic analyses of ovarian carcinoma. Nature. 2011; 474:609–15. [PubMed: 21720365]
36. Tothill RW, Tinker AV, George J, Brown R, Fox SB, Lade S, et al. Novel molecular subtypes of serous and endometrioid ovarian cancer linked to clinical outcome. Clin Cancer Res. 2008; 14:5198–208. [PubMed: 18698038]
37. van der Burg ME, Vergote I, Onstenk W, Boere IA, Leunen K, van Montfort CA, et al. Long-term results of weekly paclitaxel carboplatin induction therapy: an effective and well-tolerated treatment in patients with platinum-resistant ovarian cancer. Eur J Cancer. 2013; 49:1254–63. [PubMed: 23276720]
38. Harrap KR, Jones M, Siracky J, Pollard LA, Kelland LR. The establishment, characterization and calibration of human ovarian carcinoma xenografts for the evaluation of novel platinum anticancer drugs. Ann Oncol. 1990; 1:65–76. [PubMed: 2078487]
39. Lee CH, Xue H, Sutcliffe M, Gout PW, Huntsman DG, Miller DM, et al. Establishment of subrenal capsule xenografts of primary human ovarian tumors in SCID mice: potential models. Gynecol Oncol. 2005; 96:48–55. [PubMed: 15589579]
40. Epiney M, Bertossa C, Weil A, Campana A, Bischof P. CA125 production by the peritoneum: in-vitro and in-vivo studies. Hum Reprod. 2000; 15:1261–5. [PubMed: 10831552]
41. Goodell CA, Belisle JA, Gubbels JA, Migneault M, Rancourt C, Connor J, et al. Characterization of the tumor marker muc16 (ca125) expressed by murine ovarian tumor cell lines and identification of a panel of cross-reactive monoclonal antibodies. J Ovarian Res. 2009; 2:8. [PubMed: 19538730]

Statement of Translational Relevance

Although there have been significant advances in ovarian cancer treatment over the last three decades, cure rates are essentially unchanged. The translation of cell culture data to improve clinical outcomes is complicated by many factors and clinically-relevant models that accurately recapitulate human disease have been lacking. Herein, we present a large bank of patient-derived xenografts (tumorgrafts) which maintain physiologic and molecular fidelity to human ovarian cancer. In addition, tumorgraft response to chemotherapy is reflective of the patient experience. These models provide a means to test novel therapeutics in histologically and molecularly diverse patient surrogates in order to identify predictors of treatment response. Such a resource is a valuable tool for defining optimal patients for clinical trials.

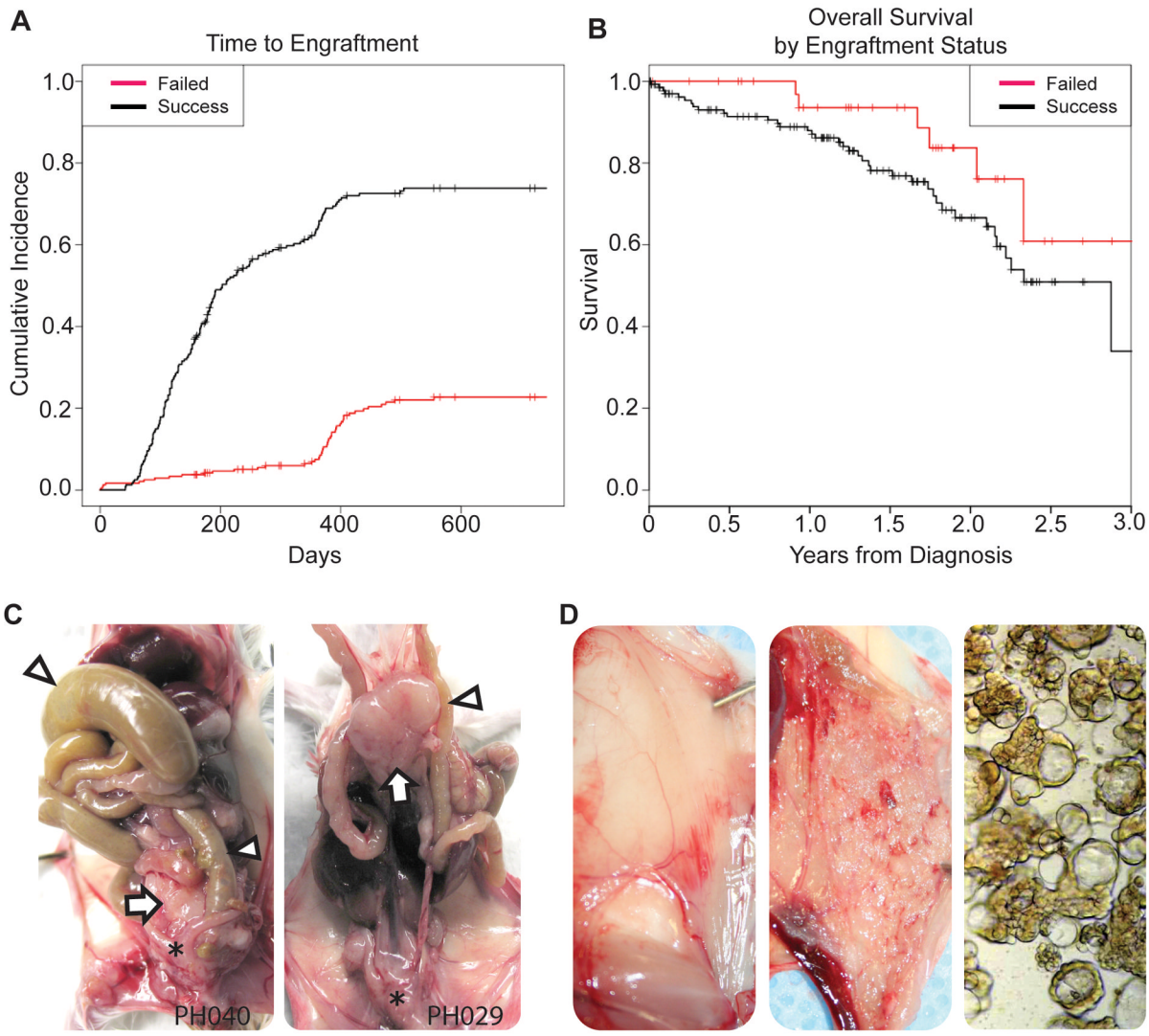

Figure 1.

Clinical correlation between tumorgraft and patient. (a) Tumorgraft engraftment rate over time where 'Success' indicates successful engraftment in at least one mouse and 'Failed' indicates failed engraftment. (b) Patient overall survival by tumorgraft engraftment status, where 'Success' and 'Failed' are as in "a". (c) Representative images from mice showing intraperitoneal dysfunction. A tumorgraft (arrow) behind the uterus (*) and caused marked bowel (triangle) obstruction (left) in one mouse but a mesenteric tumor produced non-obstructive weight loss and anorexia in another mouse (right). (d) A representative mouse with the abdominal wall reflected and showing normal, smooth-appearing peritoneum with visible vessels (left). The peritoneal surface of a mouse that developed ascites (center) demonstrates a thick cellular layer consistent with carcinomatosis. Visualization of ascitic fluid by light microscopy (right) revealed aggregates of epithelial cells (spherules).

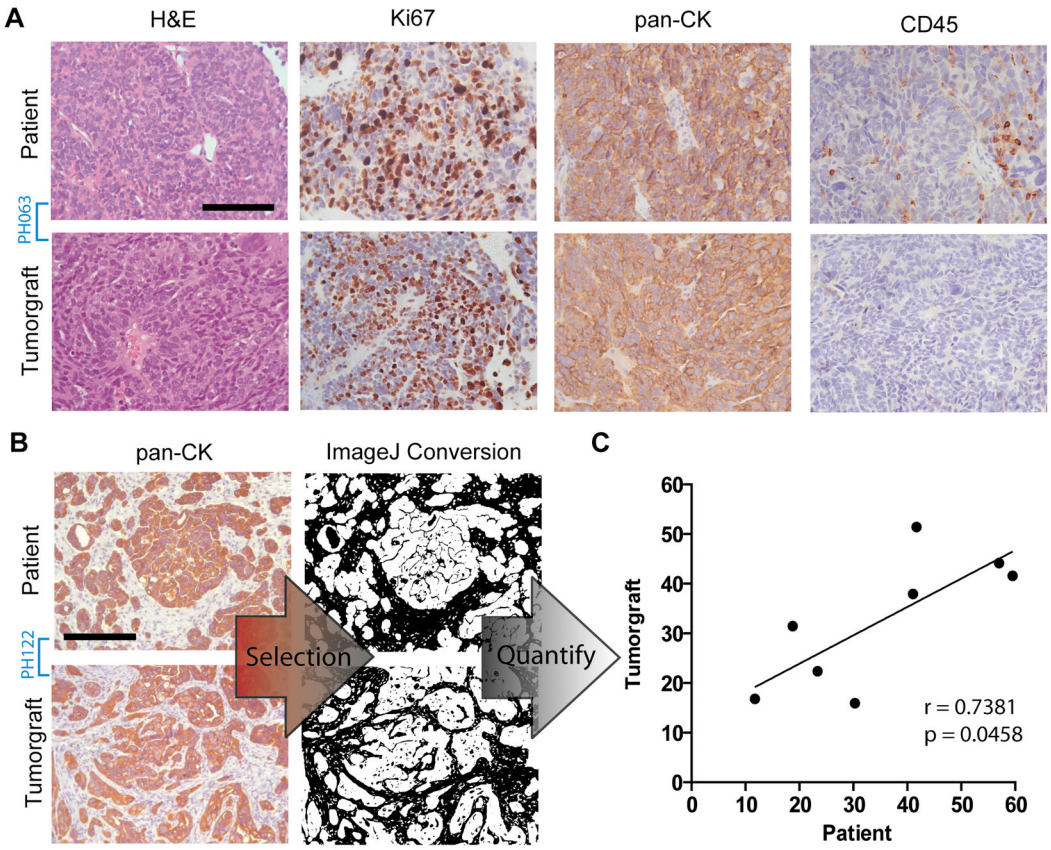

Figure 2.

Histologic similarities between patients and corresponding tumorgrafts. (a) Representative H&E, Ki67, pan-CK, and CD45 expression in tumorgraft model PH063 shows conserved morphology, proliferation index by Ki67, and epithelial phenotype by pan-cytokeratin (40x). Scale bar = 100 μm. (b) Cytokeratin staining in tumorgraft and source patient pathology sections (PH122 shown) were selected and quantified using ImageJ software as described in the Methods section (20x). Scale bar = 200 μm. (c) The calculated non-epithelial tissue for eight tumorgraft models were plotted against that of the source patient.

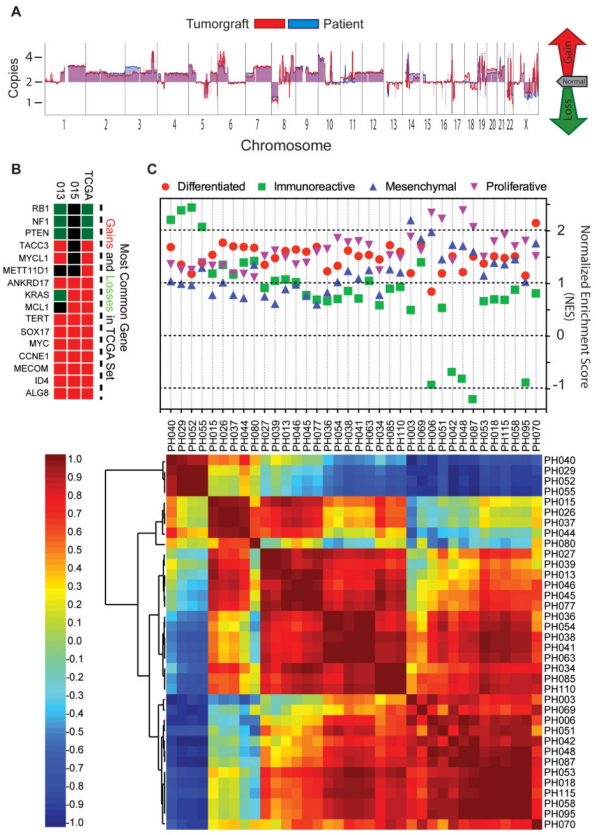

Figure 3.

Molecular analysis of tumorgrafts. (a) Graphical representation of array CGH at the chromosome level from source patient (blue) and tumorgraft (red) in model PH015 (high grade endometrioid). (b) Heat map comparison of frequently lost (green) and gained (red) genes is the TCGA dataset (right column) compared to two representative tumorgrafts (PH015 and PH013, a high grade serous). (c) The upper panel shows normalized enrichment scores (NES) of 36 tumorgrafts according to the CLOVAR (Classification of Ovarian Cancer) gene signature. Varying degrees of enrichment for signatures associated with differentiated (red circle), immunoreactive (green square), mesenchymal (blue triangle up), and proliferative (purple triangle down) molecular subtypes were observed. The lower panel shows a heat map of 36 tumorgraft models clustered as a function of their gene-expression correlation with each other. Highest (red), inverse (blue), and zero correlation was used to cluster tumorgrafts by their overall correlation.

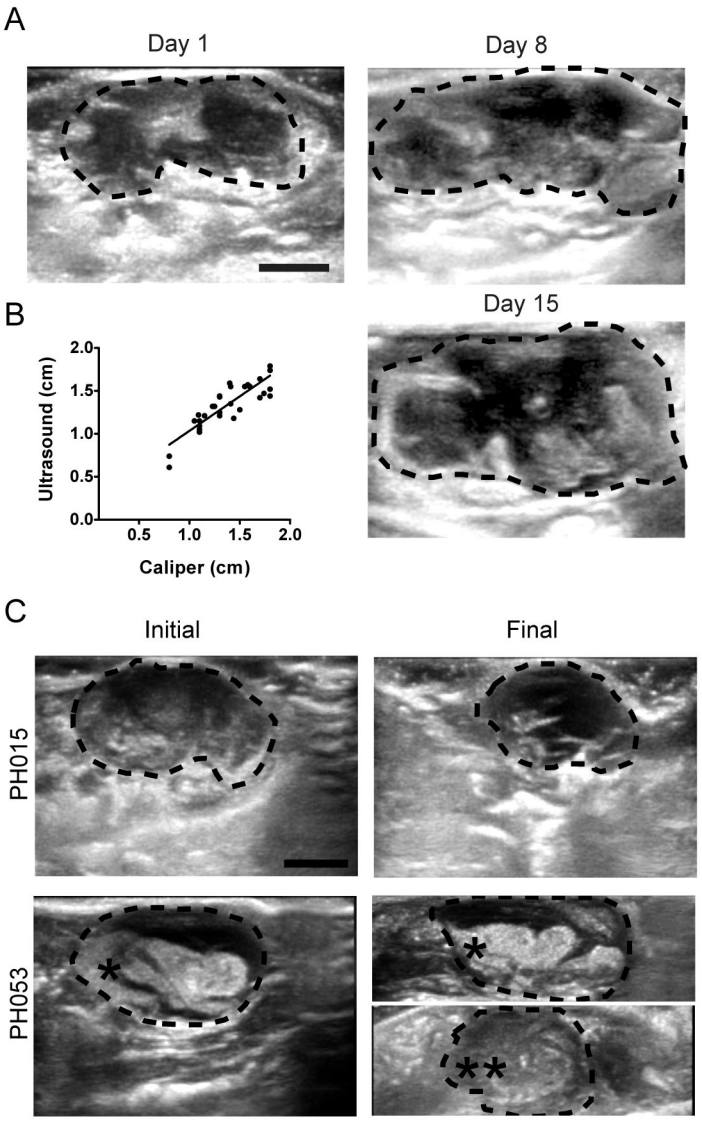

Figure 4.

Transabdominal ultrasound assessment of tumor change. (a) Representative serial ultrasound images from a saline-treated PH015 tumorgraft (dotted outline) showing growth over 15 days. (b) Tumor diameter in 32 mice bearing tumorgrafts were assessed by ultrasound and plotted against caliper-derived diameter measurements at necropsy. The Spearman correlation was high (r = 0.8491). (c) Representative tumorgraft ultrasound images showing response to treatment. A target tumor (*) was present on day 1 but a non-target tumor (**) developed during treatment. For all panels, scale bar = 5 mm and tumor cross-sectional area marked by circumferential dotted line.

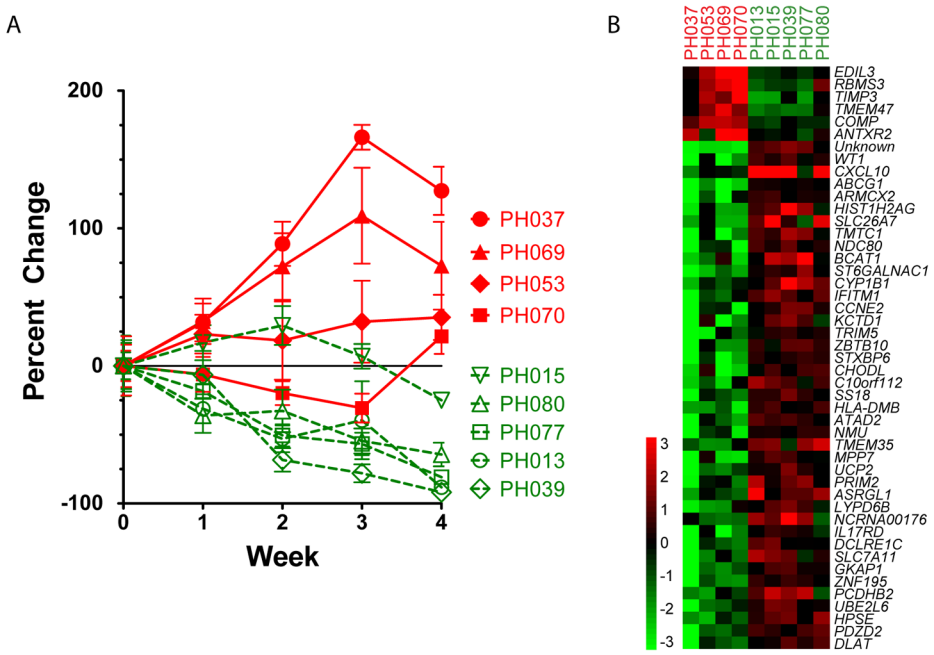

Figure 5.

Tumorgraft response to treatment with correlation to the patient experience. (a) Percent change in tumor area over time *in vivo* for tumorgraft models treated with chemotherapy. Models are derived from platinum sensitive (dotted line) or resistant (sold line) patients. (b) Heat map representing the most significantly up-regulated (red) or down-regulated (green) genes in sensitive compared to resistant tumorgrafts.

Clin Cancer Res. Author manuscript; available in PMC 2015 March 01.

Table 1

Descriptive statistics of patients providing tumor for models. FSL-Frozen section lab, which is the primary point of surgical material procurement.

	Engraftment still under assessment (Censored)	Engrafted	Failed Engraftment	All	p-value (engrafted vs. failed)
Patient age at collection, years median (range)	62 (39–89)	64 (29–91)	62 (22–85)	63 (22–91)	0.77
Time (hours) from FSL to mouse, median (range)	1.7 (1.1–2.8)	1.7 (0.9–3.6)	1.8 (0.9–7.3)	1.7 (0.9–7.3)	0.85
Morphology					
Serous	15 (63%)	111 (66%)	24 (53%)	150 (64%)	
Mucinous	2 (8%)	2 (1%)	2 (4%)	6 (3%)	
Endometrioid	1 (4%)	11 (7%)	6 (13%)	18 (8%)	
Clear Cell	1 (4%)	10 (6%)	1 (2%)	12 (5%)	
Mixed	3 (13%)	23 (14%)	4 (9%)	30 (13%)	0.018
Undifferentiated	0	1 (1%)	1 (2%)	2 (1%)	
Brenner	0	0	1 (2%)	1 (<1%)	
Carcinosarcoma	0	6 (4%)	2 (4%)	8 (3%)	
Other	2 (8%)	3 (2%)	4 (9%)	7 (3%)	
Timing of Surgery					
Primary	19 (73%)	145 (86%)	37 (82%)	201 (84%)	
Interval Debulking	0 (0%)	4 (2%)	0 (0%)	4 (2%)	0.31
Recurrent	7 (27%)	19 (11%)	8 (18%)	34 (14%)	
Stage					
I–II	4 (21%)	35 (24%)	15 (41%)	54 (27%)	0.049
III–IV	15 (79%)	109 (76%)	22 (59%)	146 (73%)	
Tumor Grade					
Borderline	1 (6%)	1 (1%)	4 (11%)	6 (3%)	0.00087
Low	4 (22%)	14 (10%)	7 (20%)	25 (13%)	
High	13 (72%)	119 (89%)	24 (69%)	156 (83%)	
Ascites					
Present	8 (44)%	77 (58%)	9 (26%)	94 (51%)	0.00091

	Engraftment still under assessment (Censored)	Engrafted	Failed Engraftment	All	p-value (engrafted vs. failed)
Absent	10 (56%)	55 (42%)	25 (74%)	90 (49%)	